Transition State Analogues for Nucleotidyl Transfer Reactions: Structure and Stability of Pentavalent Vanadate and Phosphate Ester Dianions

James Borden,[†] Debbie C. Crans,[‡] and Jan Florián*,[†]

Department of Chemistry, Loyola University Chicago, Chicago, Illinois 60626, and Department of Chemistry, Colorado State University, Fort Collins, Colorado 80523

Received: January 10, 2006; In Final Form: May 18, 2006

The structures and energy of phosphate dimethyl ester and vanadate dimethyl ester have been calculated using B3LYP/TZVP density functional quantum chemical methods and polarized continuum (PCM) and Langevin dipoles solvation models. These calculations were carried out to obtain fundamental information on the ability of vanadate esters to function as transition state analogues for the nucleotidyl transfer reaction catalyzed by DNA polymerases. Base-catalyzed methanolysis of the phosphate and vanadate dimethyl esters were the model reactions examined in this study. The structures of the phosphate and vanadate dimethyl esters and pentavalent intermediates in aqueous solution were optimized and evaluated at the PCM/B3LYP/TZVP level. The three-dimensional free energy surfaces for the studied reactions were determined at the PCM/B3LYP/TZVP//B3LYP/TZVP level. Comparison with experimental structural data obtained from the Cambridge Structural Database and with the observed kinetics of phosphate diester hydrolysis demonstrated that the level of theory chosen for these studies was appropriate. The results showed that structurally and electrostatically the vanadate dimethylester and a five-coordinate nearly trigonal bipyramidal intermediate were reasonable analogues for the parent phosphorus systems. Despite these similarities in structure, the energetics of the two systems were different, and the transition states of the two model reactions were found on different areas of the potential energy surface. When the binding energy of a transition state−DNA polymerase complex was extrapolated to a transition state analogue−DNA polymerase complex, the formation of a simple dianionic pentavalent vanadate ester adduct in the enzyme active site was not found to be sufficiently favorable. This finding suggests that additional stabilization of this adduct is needed before this type of transition state analogue will be likely to yield stable adducts with this class of enzymes. New possible candidates for such complexes are suggested.

1. Introduction

As transition state (TS) analogues, vanadium esters have been used with success to probe the reaction mechanism for a series of enzymes that catalyze the cleavage of PO bonds in the gamut of phosphate monoester, diester, and triester substrates and corresponding anhydrides.[1,2] This work focuses on the utilization of this approach with DNA polymerases. DNA polymerases,[3] an important class of enzymes facilitating DNA replication, act on deoxyribonucleoside triphosphate (dNTP) substrates that belong to the family of diester-like substrates. DNA polymerases crystallize as multicomponent complexes including protein, primer−template DNA, dNTP, and supportive metal ions[4,5] but have so far eluded attempts to crystallize complexes with transition state analogues. The reaction catalyzed by DNA polymerases is the nucleophilic attack of the primer 3′-O-riboside on the α-phosphate of dNTP. High-energy intermediates and/or transition states for DNA polymerases evolve to dianionic structures with pentavalent centers.[6,7] One possible transition state analogue structure is shown in Figure 1 with a vanadium serving as the five-coordinate center. Stabilization of these high-energy structures results from interactions with proteins and the inherent properties of a particular structural arrangement. The multitude of possible interactions as well as the richness of vanadium chemistry in aqueous solution[2] make it difficult to find the best components and conditions for a particular crystallization experiment. Therefore, more information is needed on the fundamental properties of this class of TS analogues.

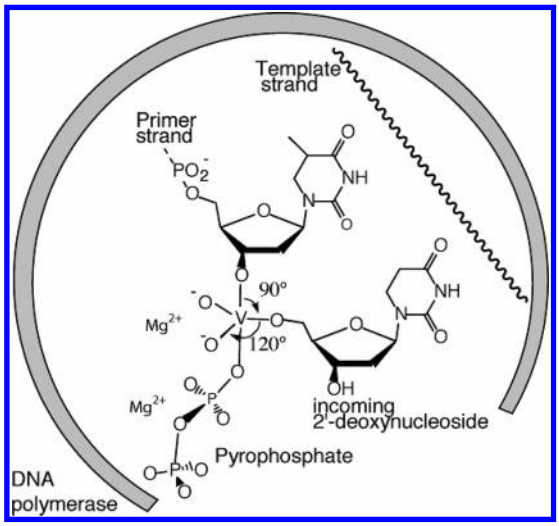

Figure 1. Possible structure of a V(V) transition state analogue in the active site of a DNA polymerase.

* Author to whom correspondence should be addressed. E-mail: jfloria@luc.edu.
[†] Loyola University Chicago.
[‡] Colorado State University.

10.1021/jp060168s CCC: $33.50
Published on Web 07/07/2006

The monoester phosphate hydrolysis in water shown in eq 1 has a maximum rate at pH 4. Hydrolysis of its monoanion is likely to follow a dissociative-type mechanism.[8−10] At neutral or higher pH the substrate is predominantly dianionic, and its hydrolysis as shown in eq 2 is significantly slower than the hydrolysis at pH 4.[11] The mechanism of the hydrolysis of phosphate monoester dianions is still under dispute, with perhaps more supporters in favor of a dissociative-type[11−13] rather than associative-type mechanism. However, it has been pointed out that most experimental evidence supporting the dissociative mechanism is also consistent with the associative mechanism.[14−17] The neutral and specific base-catalyzed phosphate diester hydrolyses shown in eqs 3 and 4, respectively, are slower than the hydrolysis of the phosphate monoester monoanion (eq 1) but faster than the hydrolysis of the dianion (eq 2). More specifically, the reaction described by eq 3 has a 38 kcal/mol activation free energy at pH 7[18,19] compared to the barriers of 31 and 44 kcal/mol for the monoester hydrolysis at pH 7 (eqs 1 and 2, respectively).[11,17]

$$H_2O + ROPO_3H^- \rightleftharpoons ROH + PO_4H_2^- \quad (1)$$

$$H_2O + ROPO_3^{2-} \rightleftharpoons ROH + PO_4H^{2-} \quad (2)$$

$$H_2O + (RO)_2PO_2^- \rightleftharpoons ROH + ROPO_3H^- \quad (3)$$

$$HO^- + (RO)_2PO_2^- \rightleftharpoons ROH + ROPO_3^{2-} \quad (4)$$

The base-catalyzed hydrolysis of the phosphate diester shown in eq 4 is the simplest model reaction for the nucleophilic attack of a deprotonated 3′-O primer on dNTP catalyzed by the DNA polymerases. The validity of the assumption that the hydrolysis of a phosphate anhydride in the dNTP molecule can be modeled by the hydrolysis of the phosphate ester has been discussed previously.[7,20−22] This reaction is likely to involve a nucleophilic attack of OH^- on a diester monoanion through an associative mechanism. The dissociative mechanism is not considered in this system because dissociation of $R'O^-$ from $ROP(O_2)OR'^-$ would generate $ROPO_2H$, i.e., alkyl metaphosphate. Alkyl metaphosphate is much less stable than metaphosphate monoanion[23−25] rendering this pathway highly unlikely. Thus, the focus of this study is to evaluate the structure of the pentavalent vanadate dianion as a potential transition state analogue for the DNA polymerase reaction.

Vanadate is recognized as an effective structural and electronic analogue of phosphate.[2] Vanadate esters are analogues of phosphate esters although this analogy is much less recognized.[26,27] Both vanadate and vanadate esters are effective inhibitors for enzymes such as ribonuclease and various phosphatases catalyzing P−O bond cleavage and formation.[2,26,27,28] Vanadium in oxidation state V has a high affinity for five-coordinate geometries resembling the high-energy five-coordinate structures of the associative phosphate ester cleavage reactions.[2] Thus, although the five-coordinate geometries may not be perfect transition state structures and provide 100% of the stabilization expected for a perfect transition state analogue,[29,30] vanadium complexes have been used with much success in kinetic and structural studies of enzyme mechanisms.[1,2,31]

The theoretical foundation for the application of vanadium(V) compounds as transition state analogues of DNA polymerases is based on the structures of dianionic pentavalent phosphate and vanadate intermediates and their reaction in aqueous solution. In this work we examine the model reaction of dimethyl phosphate ($(CH_3O)_2PO_2^-$) with methoxide and compare this reaction with the reaction of the corresponding vanadium(V) dimethyl vanadate ($(CH_3O)_2VO_2^-$) with methoxide (eqs 5 and 6).

$$CH_3O^- + (CH_3O)_2PO_2^- \rightleftharpoons (CH_3O)_2PO_2^- + CH_3O^- \quad (5)$$

$$CH_3O^- + (CH_3O)_2VO_2^- \rightleftharpoons (CH_3O)_2VO_2^- + CH_3O^- \quad (6)$$

The reaction in eq 5 is analogous to the base-catalyzed hydrolysis of $(CH_3O)_2PO_2^-$ generally described by eq 4. Earlier ab initio studies of this hydrolysis reaction in aqueous solution[7,32−37] addressed activation free energies but did not provide a complete three-dimensional free energy surface that is important for the correct identification of transition states and reaction intermediates in aqueous solution.

To properly evaluate the starting point of the reaction surface we characterize two conformers, gauche−gauche (gg) and gauche$^+$−gauche$^-$ (g^+g^-), of $(CH_3O)_2PO_2^-$ and $(CH_3O)_2VO_2^-$. The gg conformer was selected because it is the most stable conformer of $(CH_3O)_2PO_2^-$ in both gas-phase and aqueous solution[38−40] and the preferred reactant and product. In contrast, the $(CH_3O)_2PO_2^-$ g^+g^- conformer is very unstable due to the steric repulsion between the two methyl groups,[40] but this repulsion is likely to be significantly alleviated in $(CH_3O)_2VO_2^-$. We also calculate the atomic charges of the starting material and the pentavalent dianionic intermediate containing the vanadium(V) and phosphorus central atoms. Combined considerations of the structure and kinetics presented in this paper are intended to establish a firm foundation for the design of vanadate-diester-based transition state analogues for nucleic acid synthesis and hydrolysis.

2. Computational Methods

2.1. Geometries and Atomic Charges of $(CH_3O)_2PO_2^-$, $(CH_3O)_2VO_2^-$, and Pentavalent Intermediates. To examine the structural effects of replacing phosphorus by the V(V) atom we balanced the negative charge of the studied molecules by the Na^+ or Mg^{2+} counterions and optimized the geometry of the resulting neutral complex in aqueous solution by the integral equation formalism implementation of the polarized continuum model (IEF-PCM).[41] The B3LYP density functional, which consists of Becke's three-parameter hybrid gradient-corrected exchange functional[42] combined with the gradient-corrected correlation functional of Lee, Yang, and Parr,[43] and the triple-ζ valence polarized basis set of Ahlrichs (TZVP)[44] were used for these calculations. This level of theory will be further denoted as IEF-PCM/B3LYP/TZVP. The default united atom solute−solvent boundary and IEF-PCM parameters implemented in the Gaussian 03 program[45] were used. In the framework of the united atom model, the hydrogen atoms are enclosed in the sphere of the atom to which they are bonded. Thus the solution geometry of the methyl groups cannot be rigorously optimized. Therefore, we fixed the HCH bond angles at 109.5°.

The geometry of the pentavalent intermediates was optimized in two steps. First, the axial PO and VO bonds were fixed at 1.9 and 2.0 Å, respectively, and the remaining degrees of freedom were fully relaxed using loose convergence criteria (keyword opt = loose). Subsequently, the bonds, angles, and torsions defining the positions of the hydrogen atoms were fixed, and the remaining coordinates including axial PO and VO distances were optimized using the loose convergence criteria.

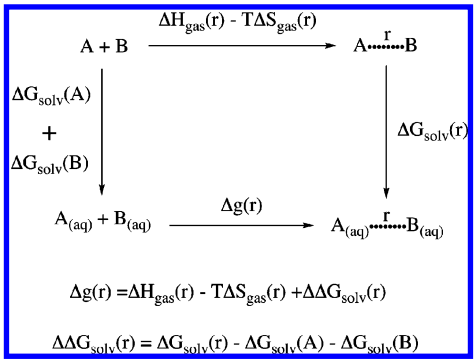

Figure 2. Thermodynamic cycle used for the calculation of the free energy ($\Delta g(r)$) surface for the reaction of A + B in solution. The symbol r denotes the reaction coordinate. Infinitely separated reactants ($r = \infty$) are denoted A + B. The top horizontal reaction corresponds to the association of reactants A and B in the gas phase. The vertical reactions correspond to the transfer of the solutes from the gas phase (1 M) to solution (1 M).

Each counterion was initially positioned along the axis originating at the P or V atom and bisecting the $^{-}O-P-O^{-}$ (or $^{-}O-V-O^{-}$) angle formed by the terminal oxygen atoms (O_t). The presence of the counterions helps to describe the arrangements in most enzyme active sites, in which the phosphate or vanadate compounds are often complexed by metal cations. Also, the geometry optimization at the PCM level is more reliable for neutral compounds than that for negatively charged solutes. Finally, because the wave function of neutral molecules is generally less diffuse, we could use a large TZVP basis set without running into problems with the electron density leaking outside the solute cavity. A flexible basis set is needed to accurately describe d-orbitals on P and V atoms that contribute significantly to the molecular wave function of pentavalent intermediates.

Atomic charges were fitted to the molecular electrostatic potential determined at the IEF-PCM/B3LYP/TZVP level. Keyword population = (mk, dipole) was used for these calculations. All quantum chemical calculations were carried out using the Gaussian 03M program.[45]

2.2. Free Energy Surfaces. To evaluate the change of the free energy of the reacting system (Δg) as a function of the reaction coordinate x in solution (i.e., $\Delta g(x)$ is a potential of mean force) we employed an approach based on the thermodynamic cycle shown in Figure 2 and described by eq 7

$$\Delta g(r) = \Delta H_{gas}(r) + \Delta\Delta G_{solv}(r) - T\Delta S_{gas}(r) \qquad (7)$$

where H_{gas}, ΔG_{solv}, S_{gas}, and T denote, respectively, the enthalpy of the isolated solute, the solute hydration free energy, the gas-phase solute entropy, and the thermodynamic temperature. The calculations were carried out for $T = 298$ K.

The magnitude of S_{gas} is frequently calculated as the sum of the translational, rotational, and vibrational entropies calculated using the ideal-gas, rigid rotor, and harmonic oscillator approximations.[46] However, it has been argued that the use of this approximation often leads to a large overestimation of the entropy term for reactions in solution.[47] There are several reasons for this overestimation. First, the harmonic approximation underestimates the entropy contribution from the low-frequency modes that are more abundant in a larger solute. Second, ΔG_{solv} calculated by implicit solvation models neglects the changes in the solute entropy upon the transfer from the gas-phase to the solution. Third, to avoid demanding ab initio calculations of vibrational frequencies, it is convenient to replace ΔH_{gas} by ΔE_{gas}. However, the neglected enthalpic contributions of vibrational and rotational modes usually compensate for a fraction of the $-T\Delta S_{gas}$ contribution. Thus, the absence of these enthalpic contributions should be accompanied by scaling down the entropy contributions.

After considering the three arguments mentioned above, we decided to calculate the free energy profile using a simplified expression

$$\Delta g(r) = \Delta E_{gas}(r) + \Delta\Delta G_{solv}(r) + 2.4 \text{ kcal/mol} \qquad (8)$$

where $\Delta E_{gas}(r)$ represents the change of the gas-phase solute energy. In the approximation of eq 8, the 2.4 kcal/mol constant can be interpreted as the entropic component of the free energy associated with moving two reacting molecules in solution, each in 1 M concentration, into a common solvent cage without restricting their mutual orientation (see, for example, eq 5 in ref 47 or page 16 of ref 48). This approach is frequently used in calculations of chemical processes in aqueous solution.[9,17,49−52]

The E_{gas} energies were calculated at the B3LYP/TZVP level. For each reaction, a series of partial geometry optimizations in the gas phase was carried out to construct the two-dimensional gas-phase potential energy surface (PES) on a grid defined by distances of the phosphorus (P) or vanadium (V) atoms to the nucleophilic (O_{nuc}) and the leaving (O_{lg}) group oxygen atoms. These distances were kept constant in each geometry optimization. The PES consisted of 13 × 14 and 14 × 15 points for the reactions involving the P and V compounds, respectively. The gas-phase energy of the reference state of infinitely separated reactants was calculated by full geometry optimization of the CH_3O^- and $(CH_3O)_2PO_2^-$ or CH_3O^- and $(CH_3O)_2VO_2^-$ molecules at the B3LYP/TZVP level. The total charge of the reacting system was −2 because we did not include Na^+ or Mg^{2+} counterions in the system. The assumed spin multiplicity of each of the reactants and of the reacting system was 1 (singlet state).

The magnitude of $\Delta\Delta G_{solv}(r)$ for use in eq 8 was evaluated using a PCM method that was calibrated to provide the same magnitude of $\Delta\Delta G_{solv}$ for the rate-limiting transition state structure as the Langevin dipoles (LD) solvation model[53] using the formula

$$\Delta\Delta G_{solv}(r) = \Delta\Delta G_{solv}(r,\text{PCM}) + \Delta\Delta G_{solv}(\text{TS,LD}) - \Delta\Delta G_{solv}(\text{TS,PCM}) \qquad (9)$$

The reason for the use of this combined approach is that the LD model is designed to include the solvent saturation effect that becomes increasingly important for highly charged solutes. Because it is impractical to calculate Langevin dipole solvation for all the grid points of our surface we assumed that the difference between the PCM and the LD relative solvation free energies is constant for the whole reaction surface and equals the difference at the transition state. We then added this constant to $\Delta\Delta G_{solv}$ calculated at the PCM level. This constant was 10.9 and 1.8 kcal/mol for the free energy surfaces for reactions 5 and 6, respectively. A smaller correction for the vanadate surface is consistent with smaller solvent saturation effects due to the larger size of the vanadate in comparison to phosphate dianions. The $\Delta\Delta G_{solv}(r,\text{PCM})$ values were calculated for each geometry corresponding to a grid point of the PES and for the reactant state using the IEF-PCM/B3LYP/6-31G* method.[41] The solute−solvent boundary was generated using Pauling's van der Waals radii (1.2, 1.4, 1.5, 1.7, and 1.8 Å for H, O, C, V, and P atoms, respectively) scaled by a factor of 1.05. This scale factor was determined to minimize the weighted

least-squares deviation of the calculated ΔG_{solv} from experimental ΔG_{solv} for CH_3O^- (-98 ± 5 kcal/mol) and HPO_4^{2-} (-245 ± 15 kcal/mol).[54] Because of the larger absolute error of the experimental ΔG_{solv} for HPO_4^{2-} the deviation for this compound was weighted by 0.33. ΔG_{solv} values calculated for CH_3O^- and HPO_4^{2-} were -87.1 and -263.5 kcal/mol, respectively. The HF/6-31G* basis set, the dielectric constant of 78.4 (water), and keywords noaddsph, pcmdoc, scfvac, and modifysph were used in these IEF-PCM calculations. A smaller 6-31G* split-valence polarized basis set was used for the calculations of ΔG_{solv} to limit the amount of negative charge escaping outside the cavity formed by the solute−solvent boundary.

3. Results and Discussion

3.1. Ground-State Properties. *3.1.1. Structures of Dimethyl Phosphate Ester.* Geometric parameters for phosphate diesters are known and have been described in detail previously.[38,40,55,56] A detailed comparison of $(CH_3O)_2PO_2^-$ in vacuo and in the solid state of $NH_4^+[(CH_3O)_2PO_2^-]$ has been carried out using Carr−Parinello DFT calculations.[57] Analysis of the chemical bonding in terms of localized Wannier orbitals showed that stereoelectronic effects are not as important as environmental effects in inducing modifications to the bond lengths to the phosphorus atom. Similar conclusions were reached in an earlier ab initio study[39] that compared gas-phase geometries of $(CH_3O)_2PO_2^-$ and $Na^+[(CH_3O)_2PO_2^-]$ at the HF, MP2, and DFT levels of theory with the X-ray geometry of barium diethyl phosphate[58] and also in the recent calculation of Mg^{2+} $[(CH_3O)_2PO_2^-]$ complexes hydrated with four or five explicit water molecules.[59] In these studies the bonds between P and terminal oxygen (O_t) atoms increased whereas the bonds between P and bridging oxygen (O_b) atoms decreased in the metal complexes. In particular, the comparison of the gas-phase and crystal structures[39,58] shows that the crystal environment increases the bond length between P and O_t from 1.50 to about 1.52 Å and shortens distances between P and O_b from 1.68 to 1.58/1.60 Å. The crystal environment widens the O_b-P-O_b angle ($\angle O_b-P-O_b$) from 100° to 104° and decreases $\angle O_t-P-O_t$ from 126° to 122°.

The parameters for the geometry of the gg conformer of the $Na^+[(CH_3O)_2PO_2^-]$ complex in aqueous solution are shown in Figure 3, top. The calculated $P-O_t$ bond length of 1.52 Å is the same as that previously reported.[39,58] The P−O bond lengths reported for the typical methyl, ethyl, and other alkyl phosphate esters range from 1.58 to 1.60 Å.[58,60−62] Although there are some small changes as the cation changes, these differences generally do not exceed 0.02 Å.[58,60−62] These observed bond lengths are shorter than the value of 1.65 Å calculated for the $(CH_3O)_2PO_2^-$ $P-O_b$ bond length. However, a few X-ray structures have been reported with $P-O_b$ bond lengths of 1.63 and 1.64 Å such as in a *p*-nitrophenyl phosphate ester[63] and in a 3′-O-uridine phosphate ester.[64] Other structural changes in the phosphate ester or elsewhere in the molecules do not generally result in significant change in the $P-O_b$ bond lengths either.[65,66] The calculated $\angle O_t-P-O_t$ and $\angle O_b-P-O_b$ were 117° and 103°, respectively. The smaller calculated $\angle O_b-P-O_b$ may partially reflect the smaller charge and ionic radius of Na^+ than Ba^{2+} as well as an improved description of the system.

3.1.2. Structures of Dimethyl Vanadate Ester. At this time there are no structural data for mononuclear vanadate monoesters or diesters. However, some information is available for vanadate triesters as well as multinuclear vanadium(V) alkoxides with one or two alkoxide (ester) groups from the Cambridge Structure Database.[67−78] Generally, the V═O bond length is around 1.57 Å, and the $V-O_b$ bond length is around 1.75 Å when the vanadium is four-coordinate.[67,69−72] However, in most alkoxide systems the triesters associate, and several X-ray structures are available for vanadium with five-coordinate geometries with the typical V_2O_2 diamond core structure.[2,73−75] In the structures with five-coordinate V(V) the V═O bond length increases slightly to about 1.59 Å, but the $V-O_b$ bond length is elongated to around 1.85 Å.[68,73−75] Examples of six-coordinate geometries as parts of other structural frameworks have also been reported.[76−78] In these structures the V═O bond length generally is around 1.58 Å, and the $V-O_b$ bond lengths vary from 1.8 to 2.0 Å.[78] Various structural features can modify these bonds as dictated by the structural framework that the unit is involved in.[76,77]

The structures for the gg and g^+g^- conformers of $(CH_3O)_2VO_2^-$ were calculated. These calculations were not meant to supplant a complete conformational analysis but rather to quantify an important difference in the conformational properties of $(CH_3O)_2VO_2^-$ and $(CH_3O)_2PO_2^-$ (see below) and underscore

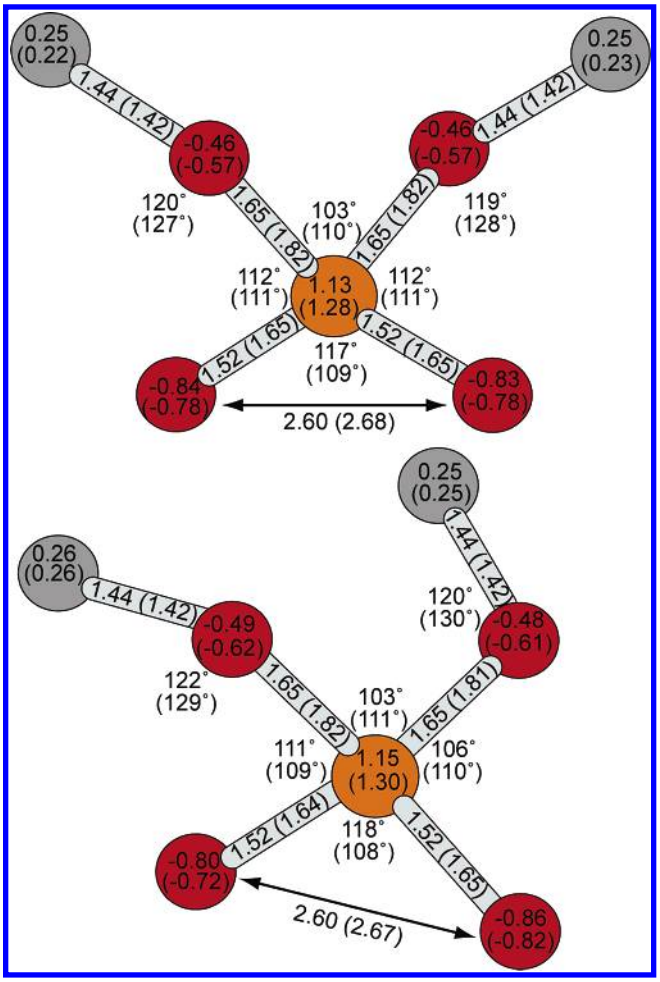

Figure 3. Calculated bond lengths (Å), bond angles (deg), and atomic charges (au) are shown for Na^+ complexes of $(CH_3O)_2PO_2^-$ and $(CH_3O)_2VO_2^-$ (data in parentheses) in aqueous solution. The data for the gg and g^+g^- conformers are shown in the top and bottom part of the figure, respectively. The phosphorus atoms and methyl groups are denoted by orange and gray spheres, respectively. The red spheres are used to denote both the bridging (O_b) and the terminal (O_t) oxygen atoms. The sodium ion and methyl hydrogen atoms are not shown. The geometries and ESP atomic charges were calculated at the PCM/B3LYP/TZVP level.

TABLE 1: Relative Free Energies of the g^+g^- Conformers of $(CH_3O)_2PO_2^-$ and $(CH_3O)_2VO_2^-$

	ΔG (kcal/mol)[a]	
method	$(CH_3O)_2PO_2^-$	$(CH_3O)_2VO_2^-$
B3LYP/TZVP	2.0	0.5
IEF-PCM/B3LYP/TZVP	1.7	0.1

[a] Relative to the free energy of the gg conformer.

the conformational dependence of the calculated structural parameters. For both conformers the V−O_t bonds are 1.65 Å and significantly longer than the V═O bonds of 1.59 Å observed in the X-ray structures of the triesters. Considering that the V−O_t bonds in the VO_2^- unit have partial double bond character, whereas the V═O bonds in the X-ray structures are full double bonds, the calculated bonds are expected to be longer than the bonds observed for triesters. We conclude that an observed elongation of 0.06 Å is reasonable. The V−O_b bond length of 1.82 Å predicted by the calculation is only slightly longer than that generally observed for the triesters. On the basis of these considerations and the recognition that only limited experimental data is available for the comparison, we conclude at this time that the level of theory applied in this work is adequately describing the vanadate dimethylester.

3.1.3. Comparison of Structures of Phosphate and Vanadate Dimethylesters. When we compare the geometries of $(CH_3O)_2PO_2^-$ and $(CH_3O)_2VO_2^-$, a few similarities and mostly differences between the two molecules are apparent. Perhaps the most striking observation is the fact that despite the differences in the P−O_t and V−O_t bond lengths the distance between the two terminal O_t atoms differs only by 0.07 Å because $\angle O_t-V-O_t$ is more acute than $\angle O_t-P-O_t$ (Figure 3, top). Consequently a protein interacting with the phosphate or vanadate derivatives will experience very similar geometric and electrostatic signatures of these molecules due to their similar atom positioning and electrostatic potential energy surfaces.

As shown by the energies calculated for each conformer there are differences in geometric parameters and conformation preferences. The V−O_t and V−O_b bonds in both the gg and g^+g^- conformers of $(CH_3O)_2VO_2^-$ are longer by 0.17 and 0.13 Å than the P−O_t and P−O_b bonds in $(CH_3O)_2PO_2^-$, respectively. In addition, there is a significant variation in the population of the conformers as reflected by the relative free energy differences for the gg and g^+g^- conformers of $(CH_3O)_2PO_2^-$ and $(CH_3O)_2VO_2^-$ (Table 1). Earlier calculations at the LD/MP2 level of theory found that the gg conformer is the most stable conformer of $(CH_3O)_2PO_2^-$ in aqueous solution, and the free energy difference between the gg and g^+g^- conformers is 2.1 kcal/mol.[40] The present $(CH_3O)_2PO_2^-$ calculation prefers the gg conformation to the g^+g^- conformation by 1.7 kcal/mol.

In contrast, the relative free energy of 0.1 kcal/mol between the gg and the g^+g^- conformers of $(CH_3O)_2VO_2^-$ suggests that none of the vanadium diester conformers are dominant but that all these conformers will exist simultaneously. The decreased stability of the g^+g^- conformer of $(CH_3O)_2PO_2^-$ is attributed to the steric repulsion between the methyl group in the smaller $(CH_3O)_2PO_2^-$ molecule, which is alleviated in $(CH_3O)_2VO_2^-$ due to the longer V−O_b bonds.

3.1.4. Charges on Dimethyl Phosphate and Dimethyl Vanadate Diesters. The electrostatic potential derived atomic charges for $Na^+[(CH_3O)_2PO_2^-]$ and $Na^+[(CH_3O)_2VO_2^-]$ complexes in aqueous solution obtained at the IEF-PCM/B3LYP/TZVP level of theory are presented in Figure 3. These charges are compared to the gas-phase charges obtained at the B3LYP/TZVP and HF/6-31G* levels in Table 1S. The HF/6-31G* method is commonly used for the generation of atomic charges for the popular Amber force field.[79] The charges on $(CH_3O)_2PO_2^-$ are more negative (higher) on the O_t atoms and less negative (lower) on the O_b atoms. The charges on P remain very similar in solution and in the gas phase, but the O_t charges become higher, and O_b charges lower in solution. A similar pattern was observed for $(CH_3O)_2VO_2^-$. Low-level HF/6-31G* charges mimic the $(CH_3O)_2PO_2^-$ charges in solution quite successfully. The performance of this method worsens for vanadate diesters, for which it significantly overestimates the positive charge on the vanadium atom and negative charges on the O_b atoms.

When comparing charges on the $(CH_3O)_2PO_2^-$ and $(CH_3O)_2VO_2^-$ systems, the central P atom was found to be slightly less positive than the V atom. The O_t atoms on $(CH_3O)_2PO_2^-$ were more negative than the O_t on $(CH_3O)_2VO_2^-$. The O_b atoms are slightly more negative in $(CH_3O)_2VO_2^-$ than in $(CH_3O)_2PO_2^-$. Overall these charge distributions suggest that electron density is shifted from the VO_2 unit to the alkoxide group in the case of $(CH_3O)_2VO_2^-$. The effect was greater for the g^+g^- conformer than that for the gg conformer. The resulting smaller dipole moment of $(CH_3O)_2VO_2^-$ would contribute to the smaller calculated ΔG_{solv} of $(CH_3O)_2VO_2^-$ (−70 kcal/mol) compared to $(CH_3O)_2PO_2^-$ (−77 kcal/mol). Presumably, the larger overall size of $(CH_3O)_2VO_2^-$ also contributes to a decrease in its ΔG_{solv}.

3.2. Free Energy Surfaces. *3.2.1. The Model Reaction for DNA Polymerases in Aqueous Solution.* Active site residues in DNA polymerases and two Mg^{2+} cations catalyze the nucleophilic attack on the α-phosphate of the substrate deoxyribonucleoside triphosphate.[3] A simple and effective model reaction for this protein reaction is the methoxide attack on $(CH_3O)_2PO_2^-$ and subsequent dissociation of the resulting high-energy intermediate.[7,18,23,80−82] Although neither CH_3O^- nor $(CH_3O)_2PO_2^-$ are close analogues of the substrate deoxyribose anion or dNTP, their reaction does embody the associative nucleophilic reaction mechanism in a P-containing substrate. Thus, despite the simplification of the DNA polymerase substrates in the model reaction, the system chosen is likely to exhibit the critical properties of this class of reactions.[7] Importantly, the reactants are of limited sizes, which are amenable to high-level ab initio calculations and allow the detailed comparison of the reactivities of $(CH_3O)_2PO_2^-$ and $(CH_3O)_2VO_2^-$.

3.2.2. Free Energy Surfaces for Methanolysis of $(CH_3O)_2PO_2^-$ and $(CH_3O)_2VO_2^-$ in 1 M Methoxide. The three-dimensional free energy profiles for the identity reactions of $(CH_3O)_2PO_2^-$ (top) and $(CH_3O)_2VO_2^-$ (bottom) are presented in Figure 4. The structures of the reactants and the products used for the generation of the free energy surfaces are detailed in Figure 3 and are shown in the center panel (below the top potential energy surface) of Figure 4. Beginning in the top surface from the reactant corner (right corner shown at 2.8 Å), the coordinate R1 corresponds to the distance between the incoming nucleophilic oxygen atom (O_{nuc}) and the P in $(CH_3O)_2PO_2^-$. From the pentavalent intermediate (the front corner at 1.85/1.85 Å) the coordinate R2 corresponds to the distance between the central P in the pentavalent intermediate and the oxygen leaving methoxide group (O_{lg}). The product is formed in the left corner of the potential energy surface with the R2 at 2.9 Å shown. The high-energy alkylmetaphosphate anion is shown in the far rear corner at 2.8/2.9 Å. Note that because the nucleophite and leaving groups are identical we assigned the R1 and R2 coordinates as P−O_{nuc} and P−O_{lg} arbitrarily. For the vanadate

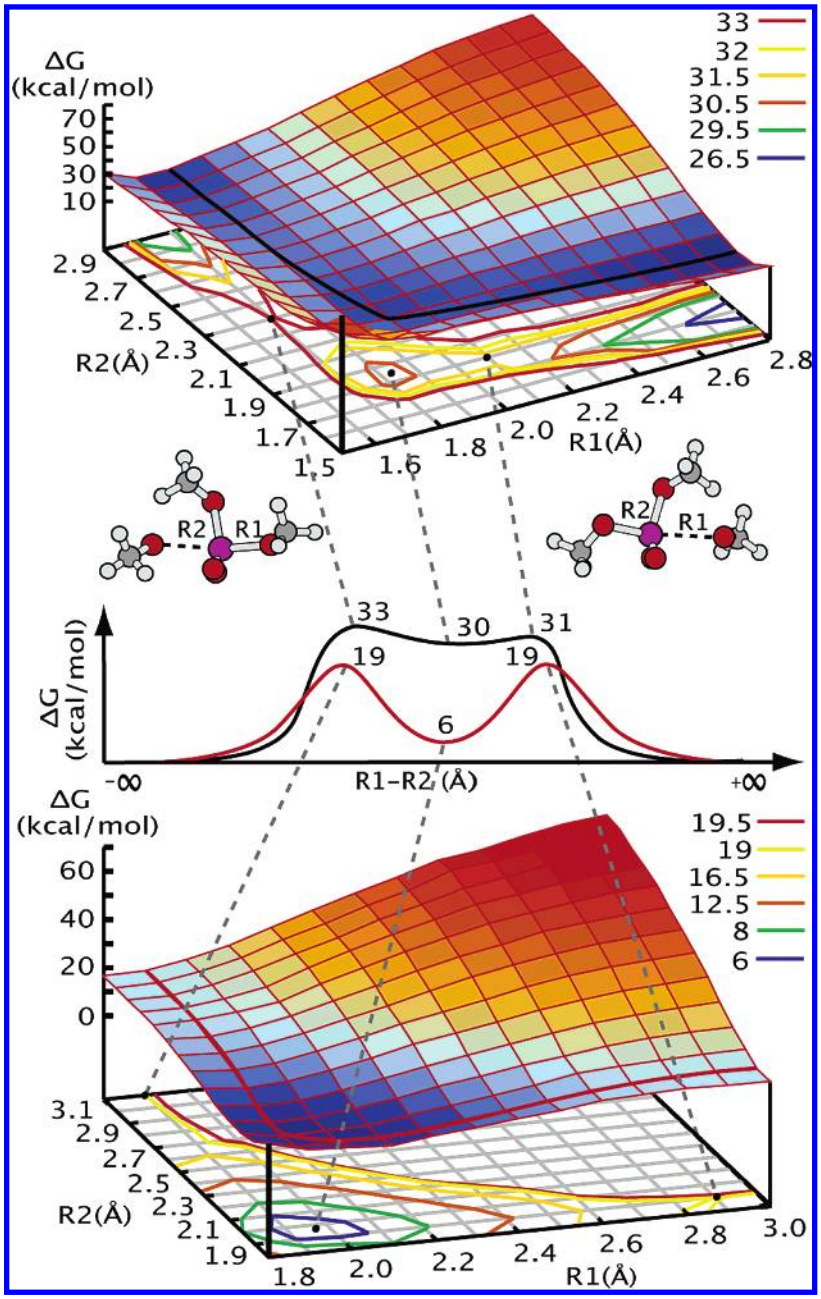

Figure 4. Free energy surface for the identity reactions $CH_3O^- + (CH_3O)_2PO_2^- \rightleftharpoons (CH_3O)_2PO_2^- + CH_3O^-$ (top) and $CH_3O^- + (CH_3O)_2VO_2^- \rightleftharpoons (CH_3O)_2VO_2^- + CH_3O^-$ (bottom). The coordinates R1 and R2 were arbitrarily chosen to correspond to the distance in angstroms from P (or V) to the O_{nuc} and O_{lg} atoms, respectively. The zero free energy level corresponds to the infinitely separated reactants or products (not shown). The isoenergetic levels are projected onto the bottom grid. The free energy surfaces were determined using eqs 8 and 9. The gas-phase energies and solvation free energies used were calculated at the B3LYP/TZVP and PCM/HF/6-31G*//B3LYP/TZVP levels, respectively. The minimum energy reaction pathway is plotted in the center of the figure in black for the $(CH_3O)_2PO_2^-$ reaction and red for the $(CH_3O)_2VO_2^-$ reaction, respectively.

dimethylester reaction the same coordinates were used with the V replacing the central P atom.

The reaction mechanism that proceeds via the far rear corner of the free energy surface is dissociative. This mechanism can be excluded because the energy of the methylmetaphosphate (CH_3PO_3) is at a maximum at about 60 kcal/mol above the reactants and products. Due to less compact geometries of the structures near the dissociative corner of the surface, our assumption that the difference between the PCM and LD solvation free energies is constant over the whole reaction surface (eq 9) is expected to lead to the overestimation of the stability of the dissociative structures by 3−5 kcal/mol, which further strengthens our conclusion about exclusion of the dissociative mechanism. This conclusion is also in agreement with the results of previous experimental[23] and quantum chemical[7,25,83] studies. Since the corresponding region of the potential energy surface for the vanadate diester reaction also has a high-energy maximum, Figure 4 (bottom), the dissociative mechanism is also excluded for this vanadate diester methanolysis reaction.

The minimum energy reaction pathways for both top and bottom free energy surfaces are shown in the two-dimensional diagram in the middle part of Figure 4. The reaction shown in black is that for the parent P-containing species, and that in red for the V-containing species, respectively. The reactions proceed via a dianionic pentavalent intermediate for both $(CH_3O)_2PO_2^-$ and $(CH_3O)_2VO_2^-$ and illustrate clearly the differences between these two species and their pathways. The pentavalent triester

TABLE 2: Activation Free Energies for the Base-Catalyzed Dimethyl Phosphate Methanolysis in Aqueous Solution Calculated Using Different Solvation Models

	ΔG_{solv} (kcal/mol)[a]					
method	CH_3O^-	$(CH_3O)_2PO_2^-$	PTP^{2-}	TS1	$\Delta\Delta G^{\ddagger}_{solv}$ (kcal/mol)	$\Delta g^{\ddagger}$ (kcal/mol)
LD[b]	−93.0	−77.1	−233.2	−228.0	−57.9	33.4
IEF-PCM[c,g]	−79.3	−68.5	−222.6	−216.3	−68.6	22.8
IEF-PCM[c,h]	−87.1	−77.1	−240.0	−233.0	−68.8	22.6
DPCM[d,g]	−81.0	−69.8	−224.0	−216.6	−65.8	25.5
OldPCM[e,g]	−104.3	−79.3	−254.3	−250.4	−66.8	24.5
CPCM[f,g]	−79.4	−68.6	−223.0	−216.8	−68.8	22.5
IEF-PCM[c,i]	−68.2	−59.6	−203.4	−196.0	−68.2	23.1
OldPCM[e,j]	−104.6	−88.3	−262.1	−258.0	−65.1	26.2
CPCM[f,i]	−68.3	−59.7	−203.8	−196.4	−68.4	22.9
CPCM[f,k]	−78.6	−67.6	−224.8	−218.4	−72.2	19.1
experiment	−98 ± 5[l]					34 ± 4[m]

[a] Solvation free energies for the reactant, intermediate, and transition state structures. The geometry for PTP^{2-} corresponds to the point r1 = 1.8, r2 = 1.8 on the top potential energy surface in Figure 4. The geometry for TS1 corresponds to the point r1 = 1.7, r2 = 2.3 on the top potential energy surface in Figure 4. All calculations were done at the HF/6-31G* level except where otherwise noted. [b] Langevin dipoles (LD) solvation model implemented in the program Chemsol 2.1.[53] Polarized B3LYP/6-31G* solute charges calculated by Gaussian 03 using the PCM-IEF options radii = pauling were used for LD calculations. The calculated solvation entropy difference, $T\Delta\Delta S^{\ddagger}_{solv}$, at 298 K was −3.9 kcal/mol. [c] Integral equation formalism PCM (the default method in Gaussian 03). [d] Default PCM version in Gaussian 98 (implemented as a deprecated feature in Gaussian 03). [e] Default PCM version in Gaussian 94 (implemented as a deprecated feature in Gaussian 98). [f] Polarizable conductor-like solvation model[112] as implemented in Gaussian 03. [g] Pauling atomic radii scaled by 1.2 and the noaddsph option. [h] Pauling atomic radii scaled by 1.05 and the noaddsph option. [i] United atom model radii (default in Gaussian 03). [j] Unscaled Pauling atomic radii (default in Gaussian 98). [k] Klamt's radii. [l] Reference 54. [m] See the text.

dianion containing P (PTP^{2-}) is of high energy and kinetically unstable with only a 1 kcal/mol barrier toward dissociation. In contrast, the corresponding intermediate containing the five-coordinate V(V) atom (PTV^{2-}) is only 6 kcal/mol higher in free energy than the reactant state. This thermodynamically stable species is separated from the four-coordinate vanadate species by an activation barrier of 13 kcal/mol. Since standard states are assumed in these calculations at a 1 M concentration of CH_3O^- (i.e., at about pH 16) PTV^{2-} forms from $(CH_3O)_2VO_2^-$ at these conditions in a process described by an equilibrium constant of 4×10^{-5}. The lifetime of this intermediate is about 1 ms at ambient temperature and thus sufficiently long-lived for detection should it be present at a measurable concentration. These figures clearly show an important difference between the two systems.

As expected the free energy surfaces in Figure 4 feature significantly larger barriers for the methoxide attack on $(CH_3O)_2PO_2^-$ (33 kcal/mol) than on $(CH_3O)_2VO_2^-$ (19 kcal/mol). Previously, Uchimaru et al. were able to locate a TS and the PTP^{2-} intermediate on the energy profile of the reaction involving the attack of methoxide on $(CH_3O)_2PO_2^-$ in the gas phase and water clusters as a function of the $P-O_{nuc}$ and $P-O_{lg}$ distances at the Hartree−Fock level using the 3-21G* basis set.[20−22] These authors identified the conformations of the methyl groups to be key to the location and energy of a pentavalent dianion species on the energy surface. Although such conformational effects are significantly smaller in aqueous solution than those in the gas phase, we attribute the 2 kcal/mol difference in the free energies of the two transition states separating PTP^{2-} from the reactant and product valleys to such conformational changes (Figure 4). Because of longer VO bonds, steric and electronic effects of the methyl group orientation on the free energy surface of the $(CH_3O)_2VO_2^-$ reaction are smaller than those for $(CH_3O)_2PO_2^-$ reaction. These results are consistent with the larger conformational flexibility of $(CH_3O)_2VO_2^-$ than that of $(CH_3O)_2PO_2^-$ discussed in section 3.1.

The activation free energy of 33 kcal/mol for the reaction shown in eq 5 was calculated under standard conditions of 1 M CH_3O^- and 298 K. This barrier is close to a barrier of 34 kcal/mol[7] calculated at the MP2/6-31+G**//HF/6-31G* level using the LD solvation model.[54] Furthermore, a 33.6 kcal/mol barrier was calculated by Takeda et al.[34] at the B3LYP/6-31+G*//HF/6-31+G* level where the solvation effects were incorporated by the PCM method. Recently, a higher activation free energy of 37.3 kcal/mol was calculated by Iche-Tarrat et al.[37] who used the B3LYP density functional and the multipole expansion (MPE) continuum solvation model.[84,85] To overcome problems with overestimated gas-phase entropies obtained using the harmonic approximation (see also discussion of eq 7 in section 2), Iche-Tarrat et al. arrived to their calculated activation free energy by combining the MPE + B3LYP activation enthalpy with the experimental value of activation entropy, $T\Delta S^{\ddagger} = -7.3$ kcal/mol at 298 K, reported by Williams and Wyman.[81] Since all continuum solvation models including the MPE model are parametrized to calculate solvation free energies rather than solvation enthalpies[85] and the authors report using "standard MPE calculations" it is very likely that the MPE + B3LYP activation enthalpy reported by Iche-Tarrat et al. was contaminated by the solvation entropy contribution, $T\Delta\Delta S^{\ddagger}_{solv}$. We estimate, using the LD solvation model, that the magnitude of this contribution amounts to −3.6 kcal/mol at 298 K (Table 2). Since both the experimental activation entropy and the MPE + B3LYP activation enthalpy calculated by Iche-Tarrat et al. included the $T\Delta\Delta S^{\ddagger}_{solv}$ contribution, their activation free energy of 37.3 kcal/mol is about 3.6 kcal/mol larger than the activation free energy that they would have obtained using a consistent approach. The resulting consistent activation free energy would fall in the 33−34 kcal/mol range, which agrees with our current result and with the results of the other two ab initio calculations[7,34] discussed in this paragraph.

Through the use of transition state theory,[86] the calculated activation free energy of 33.4 kcal/mol can be converted to the rate constant of 2×10^{-12} M^{-1} s^{-1}. This rate constant is in good agreement with the estimate of Guthrie of 7×10^{-12} M^{-1} s^{-1},[87] which was obtained by extrapolating early kinetic data of Kumamoto and Westheimer[88] and Bunton[89] observed for $(CH_3O)_2PO_2^-$ hydrolysis at high temperatures. Because $(CH_3O)_2PO_2^-$ hydrolysis occurs predominantly by the nucleophilic attack on carbon rather than on phosphorus[18,89] it is very difficult to

TABLE 3: Activation Free Energies for the Base-Catalyzed Dimethyl Vanadate Methanolysis in Aqueous Solution Calculated Using Different Solvation Models

	ΔG_{solv} (kcal/mol)[a]					
method	CH_3O^-	$(CH_3O)_2VO_2^-$	PTV^{2-}	TS2	$\Delta\Delta G^{\ddagger}_{solv}$ (kcal/mol)	$\Delta g^{\ddagger}$ (kcal/mol)
LD[b]	−93.0	−72.9	−219.7	−218.8	−52.9	18.8
IEF-PCM[c]	−87.1	−70.1	−215.1	−211.9	−54.7	17.0

[a] Solvation free energies for the reactant, intermediate, and transition state structures. The geometry for PTV^{2-} corresponds to the point r1 = 2.0, r2 = 2.0 on the bottom potential energy surface in Figure 4. The geometry for TS2 corresponds to the point r1 = 2.9, r2 = 1.9 on the bottom potential energy surface in Figure 4. [b] LD method (Chemsol 2.1).[53] Polarized B3LYP/6-31G* solute charges calculated by Gaussian 03 using the PCM-IEF options radii = pauling were used for the LD calculations. The calculated solvation entropy difference, $T\Delta\Delta S^{\ddagger}_{solv}$, at 298 K was −4.8 kcal/mol. [c] IEF-PCM (the default method in Gaussian 03) using Pauling atomic radii scaled by 1.05 and the noaddsph option.

measure the actual rate constant for this reaction. Therefore, Williams and co-workers eliminated the attack on carbon by studying the hydrolysis of a phosphate diester with neopentyl groups at temperatures ranging from 150 to 260 °C.[19,81] The extrapolation of these experiments to the room temperature led to a slower reaction with a rate constant of 10^{-15} M^{-1} s^{-1} (at 25 °C), which corresponds to an activation free energy of 37.6 kcal/mol. However, Takeda et al.[34] observed hydrolysis of thymidyl(3′−5′)thymidine at pH 14 and 80 °C with a rate constant that can be extrapolated to the activation free energy of about 31 kcal/mol for $(CH_3O)_2PO_2^-$ hydrolysis at 25 °C. However, the validity of the interpretation of the kinetic experiments of Takeda et al. has been recently disputed by Williams and co-workers,[19] who pointed out that an opening of the thymine ring may facilitate mechanistic pathways for further decomposition of thymidyl(3′−5′)thymidine that are not available to simple phosphodiester substrates.

The experimental activation free energy of 37.6 kcal/mol,[19,81] which at present appears to be obtained by the most reliable experimental procedure, is about 4 kcal/mol higher than the calculated barrier of 33.4 kcal/mol. Since several assumptions were involved in the determinations of both the experimental and calculated free energies it is difficult to point to one of these numbers as more accurate. First, the experimental free energy at 298 K was derived by assuming that the activation entropy is constant over a wide temperature range. Given the large magnitude of the observed activation entropy[19,81] even a small deviation from this approximation could lead to a notable change of the activation free energy. Second, the steric effects of bulky neopentyl groups of the substrate could increase the barrier compared to the methyl groups of $(CH_3O)_2PO_2^-$. Third, the reaction with the methoxide (eq 5) studied computationally might be slightly faster than the reaction with the hydroxide (eq 4), which was studied experimentally. Although each of these effects is likely not to exceed 1−2 kcal/mol they might add up to cause the 4 kcal/mol difference between the calculated and observed activation free energy. Last but not least there are numerous weaknesses of the theoretical methodology that could affect the calculated activation free energy by a total error of up to 5 kcal/mol. These weaknesses include, among others, the approximation of eq 8, limiting the reaction surface to two dimensions while optimizing the remaining degrees of freedom in the gas phase rather than in solution, replacing water molecules by a continuum dielectric in the PCM model or by point dipoles in the LD model, and errors due to the approximations used in solving the Schrödinger equation. Considering all these factors the obtained agreement between the results of the first principles calculations and the experiment is very reasonable. This agreement allows us to gain confidence about the accuracy of the free energy surface for the corresponding vanadate surface, for which there are no available experimental data. Furthermore, we would like to emphasize that calculating reliable free energies is a significantly more demanding (and thus often avoided) task than obtaining sufficiently informative geometries. However, it is the knowledge of the system energetics, or more precisely free energy surfaces, that can empower the theory to make predictions for complex biologically relevant systems.

3.2.3. Transition State Geometry. The first of the two TSs calculated for the phosphorus-containing system in solution is located at a $P-O_{nuc}$ distance of 2.1 Å and $P-O_{lg}$ distances of 1.8 Å. The second TS was found for the axial P−O distances of 1.7 and 2.3 Å, respectively (Figure 4, top). The corresponding TS for the vanadium-containing system is located at significantly longer V−O distances of about 2.9 and 1.9 Å and 1.9 and 3.1 Å (Figure 4, bottom). Note, that there is about 0.1 Å uncertainty in the TS bond length because of the 0.1 Å grid spacing used to generate the free energy surface in solution. Considering that the V−O single bond length is about 0.2 Å longer than the P−O bond length (Figure 3), the comparison of the $P-O_{lg}$ and $V-O_{lg}$ bond lengths of the second TS suggests that there is a greater degree of bond breaking in the TS for the $(CH_3O)_2VO_2^-$ reaction than in the corresponding TS for the $(CH_3O)_2PO_2^-$ reaction. This observation is consistent with the Hammond postulate by which the geometry of the TS is closer to the geometry of the more unstable intermediate, which in this case is PTP^{2-}.

3.2.4. Pentavalent Reaction Intermediates. The reaction coordinates for reactions 5 and 6 pass through pentavalent dianionic intermediates derived from $(CH_3O)_2PO_2^-$ or $(CH_3O)_2VO_2^-$. Whereas PTP^{2-} is of high energy and kinetically unstable, PTV^{2-} is much more stable (Figure 4). The greater PTV^{2-} stability likely reflects a smaller energy gap between the occupied s- and p-orbitals of the vanadium(V) and its unoccupied d-orbitals than that for phosphorus with the same oxidation number. Thus V(V) may more easily expand its coordination sphere by accepting ligand electrons to its empty d-orbitals and to form sp^3d hybrid orbitals. In these hybrid orbitals, the maximum of the radial electron density is shifted farther from the atom nucleus. This shift allows V(V) to form longer covalent bonds. The longer bond distances help to further stabilize PTV^{2-} by increasing interligand separation, which results in a smaller steric and electrostatic repulsion among negatively charged ligands in PTV^{2-} than that in PTP^{2-}.

The larger electrostatic repulsion in PTP^{2-} is compensated for by a more favorable magnitude of $\Delta\Delta G_{solv}$ for PTP^{2-} due to the smaller size of PTP^{2-} than PTV^{2-} (Tables 2 and 3). However, this solvation effect is rather difficult to accurately quantify using continuum solvation models because these models are usually parametrized for neutral molecules and, to a lesser extent, for monoanions and monocations but not for molecular ions with charges +2 or −2 au. Moreover, the solvent polarizatiom (reaction field) obtained by continuum models increases linearly with the electrostatic field of the solute whereas the polarization of discrete water molecules levels off

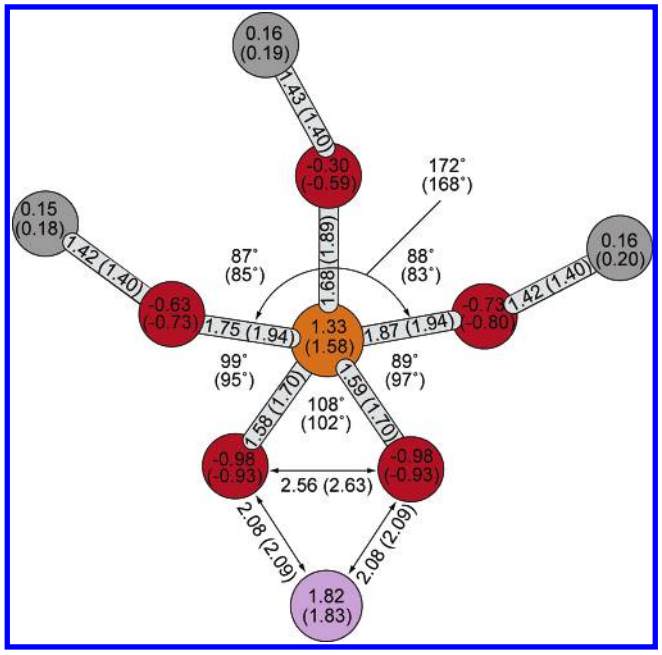

Figure 5. Comparison of bond lengths (Å), bond angles (deg), and atomic charges (au) for the Mg^{2+} complex of the pentavalent trimethyl phosphorane intermediate (PTP^{2-}) of the identity reaction $CH_3O^- + (CH_3O)_2PO_2^- \rightleftharpoons (CH_3O)_2PO_2^- + CH_3O^-$ and the Mg^{2+} complex of the corresponding V(V)-containing intermediate (PTV^{2-}) for the reaction $CH_3O^- + (CH_3O)_2VO_2^- \rightleftharpoons (CH_3O)_2VO_2^- + CH_3O^-$ (data in parentheses) in aqueous solution. The geometries and ESP atomic charges were calculated at the PCM/B3LYP/TZVP level. The phosphorus and magnesium atoms and methyl groups are denoted by orange, purple, and gray spheres, respectively. The red spheres are used to denote both the bridging (O_b) and the terminal (O_t) oxygen atoms. The methyl hydrogen atoms are not shown.

for high fields. Our earlier estimates using the LD solvation model indicated that the saturation of the solvation response becomes noticeable for small ions that carry ±2 or higher charges.[54] The absence of this saturation effect in PCM models may be the reason PCM methods yield a more negative solvation contribution to the activation free energy ($\Delta\Delta G^{\ddagger}_{solv}$) than the LD model (Table 2). Interestingly, all attempts to make ΔG_{solv} for the TS less negative by increasing the size of the solute cavity or changing other PCM parameters tend to decrease also $|\Delta G_{solv}|$ for the reactants, so no improvement in $\Delta\Delta G^{\ddagger}_{solv}$ is obtained (Table 2). The discrepancy between $\Delta\Delta G^{\ddagger}_{solv}$ results obtained by PCM and LD solvation models practically disappears for reaction 6 (Table 3). This result is consistent with a lesser importance of saturation effects for larger vanadium-containing dianionic species.

The geometry and atomic charges of the pentavalent species complexed by Mg^{2+} cations (PTP^{2-} and PTV^{2-}) and their structural and electronic details are visualized in Figure 5. Both intermediates have slightly distorted trigonal bipyramidal geometry. The distortion from the ideal trigonal bipyramidal geometry of 180° (characterized by $O_{nuc}-P-O_{lg}$ and $O_{nuc}-V-O_{lg}$ angles of 172° and 168°, respectively) is larger in PTV^{2-} than that in PTP^{2-}. The distances between the O_t-O_t atoms (2.56 and 2.63 Å) are similar in both PTP^{2-} and PTV^{2-} as are their distances to the Mg^{2+} atoms. Although more electron density in PTV^{2-} is transferred from O_t and V atoms to O_b atoms, each O_t atom still carries a large negative charge of −0.93 au. The greatest electronic difference between the PTP^{2-} and the PTV^{2-} intermediates relates to the methoxide group in the same plane as the VO_2 unit. The O_b atom of this group has a charge of −0.59 au whereas the charge of the corresponding atom in PTP^{2-} is −0.3 au. This difference likely reflects more covalent character of this equatorial $P-O_b$ bond. In contrast, the axial $P-O_b$ bonds are mostly ionic in nature, and their marginal stability (about 1 kcal/mol, Figure 4) is due to the solvation effects rather than due to the bond strength per se. Considering all the structural aspects and electronic aspects of this intermediate, there is a high degree of similarity between the PTP^{2-} and PTV^{2-} intermediates. This structural similarity makes the PTV^{2-} analogue well suited to function as a TS analogue for many reactions involving associative nucleophilic attack on phosphate diesters and anhydrides.

The calculated similarity of the geometries of PTV^{2-} and PTP^{2-} in solution is in contrary to results of the previous ab initio calculations of Krauss and Basch[90] who found the geometry of $VO_2(OH)_3^{2-}$ to be substantially distorted from the trigonal bipyramid. In particular, the calculated angle between the two axial bonds, ∠HO−V−OH, was 148° whereas the corresponding angle $\angle O_{nuc}-V-O_{lg}$ in our study is 168° (Figure 5). These geometric differences can be attributed to a different chemical composition of the two model systems ($PTV^{2-}\cdot Mg^{2+}$ in aqueous solution versus $VO_2(OH)_3^{2-}$ in the gas phase) and different methods used to calculate the electronic structure and atomic charges. However, the single most important factor causing the distortion of the structure of the $VO_2(OH)_3^{2-}$ dianion from the trigonal bipyramid was likely the presence of strong intramolecular hydrogen bonds in this dianion. A similar distortion was calculated for the pentavalent ethylene oxovanadate mono- and dianions in the gas phase.[91] In these cyclic compounds, which served as models for the structure of uridine vanadate bound to ribonuclease A, one axial and one equatorial ligand were interconnected by the ethylene bridge. The observed distortion was likely caused by the presence of this bridge.

Both previous theoretical studies[90,91] calculated the structure of the models of TS analogues in the gas phase. Since the active sites of the enzymes catalyzing phosphoryl and nucleotidyl transfer reactions are very polar and often contain divalent metal cations, we believe that the environment faced by bound TS analogues is better represented by solvated zwitterions such as that shown in Figure 5.

The fact that the presence or absence of intramolecular hydrogen bonds in the gas phase may affect the angles of axial ligands in pentavalent V(V) dianions by as much as 20° indicates a large deformational flexibility of these species. The PTV^{2-} species are also more flexible than PTP^{2-} for the rotation about C−O bonds. This difference is attributed to shorter P−O bonds that allow the distance between atoms on adjacent methyl groups to become shorter than these atoms' van der Waals radii, whereas the longer V−O bonds keep the methyl groups more separated.

3.2.5. Affinity of the PTV^{2-}-Based TS Analogues for DNA Polymerases. The calculated geometric and charge complementarily of PTV^{2-} to PTP^{2-} and its angular and torsional flexibility allow qualitative rationalization of observed high affinities of multiple enzymes for vanadate and its derivatives.[1,2] Quantitatively, this affinity is characterized by the standard free energy for the formation of an enzyme complex with a given TS analogue, $\Delta G_{E\cdot TSA}$. For TS analogues based on pentavalent V(V) ester dianions, which are a less stable form at standard conditions, it is useful to decompose $\Delta G_{E\cdot TSA}$ into the free energy of the TS analogue in aqueous solution (ΔG_{aq}) and the binding free energy of this analogue (ΔG_{bind}^{TSA}) by using the thermodynamic cycle of Figure 6. Using the calculated free energy for reaction 6 (Figure 4) and the experimental pK_a constant for methanol (15.6)[92] we can estimate the magnitude

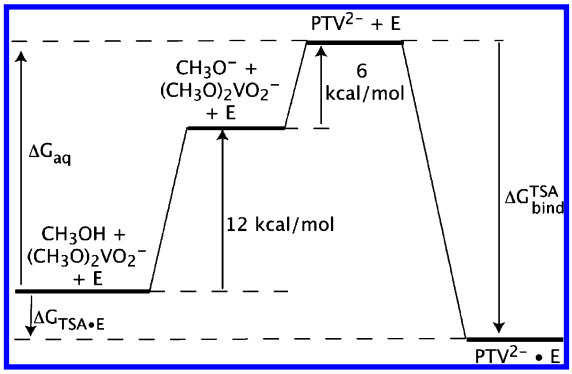

Figure 6. Thermodynamic cycle for binding of the PTV^{2-}-based TS analogue to an enzyme at pH 7.

of ΔG_{aq} for pentavalent V(V) ester dianions at pH 7 to be about 18 kcal/mol (Figure 6). The magnitude of ΔG_{bind}^{TSA} must be smaller (in absolute value) than the binding free energy for the correct (i.e., non-vanadate) TS, ΔG_{bind}^{TS},[93] which can be expressed at 298 K as

$$\Delta G_{bind}^{TS}\,(\text{kcal/mol}) = 1.36 \log(k_{non}K_M/k_{cat}) \qquad (10)$$

where k_{non}, K_M, and k_{cat} denote the rate constant for the uncatalyzed reaction in water, dissociation constant of the substrate, and the catalytic rate constant, respectively.[94] Because the typical experimental kinetic parameters for DNA polymerases are $k_{non} = 10^{-9}$ M^{-1} s^{-1}, $k_{cat} = 10^{2}$ s^{-1}, and $K_M = 10^{-5}$ M (see, for example, refs 7, 95, and references therein), ΔG_{bind}^{TS} for DNA polymerases can be estimated as −22 kcal/mol. Because the binding of any TS analogue must be weaker than binding of the true TS (i.e., $\Delta G_{bind}^{TSA} \geq \Delta G_{bind}^{TS}$), we can estimate the lower limit for the free energy of the enzyme−TS analogue complex as $\Delta G_{E\cdot TSA} = \Delta G_{aq} + \Delta G_{bind}^{TSA} \geq \Delta G_{aq} + \Delta G_{bind}^{TS} = -4$ kcal/mol. However, $\Delta G_{E\cdot TSA} < -6$ kcal/mol would be required to observe a significant fraction of E·TSA complexes at the usual working polymerase (sub-millimolar) and vanadate (<0.1 M) concentrations. Thus, the calculated stability of PTV^{2-}, which is a model for the general class of TS analogues based on acyclic pentavalent V(V) ester dianions (see, for example, Figure 1), does not support the formation of DNA polymerase−TS analogue complexes at observable concentrations.

A 2 kcal/mol difference between the lowest achievable $\Delta G_{E\cdot TSA}$ of −4 kcal/mol and $\Delta G_{E\cdot TSA}$ of −6 kcal/mol, which is required for forming an observable amount of enzyme−TS analogue complexes, may seem to be small in view of the error bars of the energetic components that enter the thermodynamic cycle of Figure 6. However, the actual $\Delta G_{E\cdot TSA}$ will be likely significantly larger than its limiting value of −4 kcal/mol, which may occur only for the extreme case of TS analogue binding affinity being identical to the affinity of the true TS.

It should be noted that the thermodynamic cycle in Figure 6 should be applicable to other enzymes and will be a topic of future work. At this time, we demonstrate the power of this method by one such example. The first step is to obtain appropriate energetic parameters for the cycle, which may be often obtained by simple adjustments. Importantly, the energetics of protonated PTV^{2-} ($HPTV^{1-}$) need to be considered to assess the affinity of ribonuclease A to vanadate diesters.[91] A pK_a value of 12 can be estimated for $HPTV^{1-}$. This estimate is based on the calculated pK_a of 10 for the corresponding phosphorane,[96] which we increased by two units to take into account the average

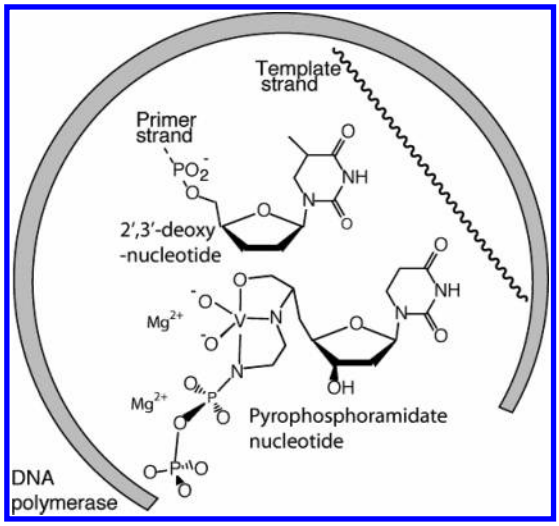

Figure 7. Proposed cyclic V(V) TS analogue in the active site of a DNA polymerase.

shift of the observed pK_a constants of vanadate esters compared to the pK_a values of corresponding phosphate esters.[8,97] Thus, the magnitude of ΔG_{aq} needs to be lowered for $HPTV^{1-}$ to 11 kcal/mol. (A possible additional decrease of ΔG_{aq} due to the formation of a cyclic variant of $HPTV^{1-}$ is, for the sake of simplicity, not considered.) By adding $\Delta G_{aq} = 11$ kcal/mol to ΔG_{bind}^{TS} of −20 kcal/mol, which was determined using experimental ribonuclease A kinetic parameters,[98] we obtain $\Delta G_{E\cdot TSA} \geq -9$ kcal/mol. This value stands in contrast to the much higher value for DNA polymerase and is consistent with the experimental observation of the ribonuclease A−vanadate crystal structure.

Apart from the likely ineffective approach depicted in Figure 1, is there any alternative strategy for the design of vanadium-containing TS analogues for DNA polymerases? Assuming that dianionic character and trigonal bipyramidal geometry for a good TS analogue for DNA polymerases must be maintained, increased solution stability of this analogue is needed. Several approaches can be taken within these structural constrains. One approach involves multidentate ligands and the stability obtained by the formation of cyclic esters[73−75,99] and amines.[100] One such possible TS analogue is shown in Figure 7. Complexes formed with ethanolamine-derivatized ligands have been characterized in detail.[101−105] The structural motif illustrated in Figure 7 has precedent since an adduct between vanadate and (2-aminoethyl)-ethanolanime was observed.[100] Detailed studies with the diethanolamine-type ligands showed that the vanadium(V) with these ligands remain five-coordinate. Additional stabilization of cyclic vanadate adducts has previously been reported in a study with glucose 6-phosphate dehydrogenase where the 1000-fold enhanced affinity for NAD + vanadate was attributed to the formation of a cyclic NADV complex that is structurally similar to c-2′3′-NADP.[106,107]

Another promising approach is to design a TS analogue based on vanadium(IV) chemistry. Although the O,N,N-donor structural motif has been characterized in detail in a range of vanadium(IV) systems, few of them maintain the five-coordinate geometry around the vanadium.[2,102,108−110] As demonstrated in studies with the ethanolamine-based ligands and vanadium(V), the coordination number around the vanadium atom is very sensitive to the nature of the substituents. When the CH_2OH group is substituted by a COOH group the vanadium becomes six-coordinate.[103,111] We are currently exploring the properties of potential transition state analogues based on vanadium(IV)

chemistry. Regardless of the final outcome, ab initio calculations in solutions accompanied by thermodynamic considerations represent an effective way to understand systems that are difficult to evaluate experimentally and provide assistance in the modification of experimental approaches based on TS analogues.

4. Conclusions

The work reported here examined the structural and electronic similarities of both the ground state and the TS in the framework of the potential energy surfaces of the alkaline methanolysis of $(CH_3O)_2PO_2^-$ and $(CH_3O)_2VO_2^-$. Despite the differences in bond lengths, we found that due to a change in angles the PTP^{2-} and PTV^{2-} structures had negatively charged nonbridging oxygen atoms at almost identical locations, thus providing similar electrostatic and steric signatures for the two species. This fact, combined with the flexibility of the coordination chemistry of the V atom, defines the vanadium as an excellent structural TS analogue from the point of matching a protein surface with the V derivative compared to that of the natural substrate's TS. When the potential energy surfaces for the P and V species were compared, dramatic differences were observed, and unless the binding stabilization by the enzyme overcame the low stability of the V compound in solution the overall enzyme−TS analogue complex may not be formed in observable quantities. Indeed, specifically considering a PTV^{2-}-like vanadate complex in a DNA polymerase, the energetics were not found to be favorable.

Acknowledgment. D.C.C. and J.F. thank the National Institutes of Health (Grant No. 1U19CA105010) for funding. Additional support was provided by a Research Corporation Research Innovation grant (to J.F.). We also thank Myron F. Goodman, Samuel H. Wilson, Lars Pedersen, William Beard, Surya Prakash, Charles McKenna, Arieh Warshel, and Alvin A. Holder for stimulating discussions.

Supporting Information Available: Cartesian coordinates, energies, and PCM/B3LYP/TZVP, B3LYP/TZVP, and HF/6-31G* atomic charges of $(CH_3O)_2PO_2^-$, $(CH_3O)_2VO_2^-$, PTP^{2-}, and PTV^{2-}. This material is available free of charge via the Internet at http://pubs.acs.org.

References and Notes

(1) Davies, D. R.; Hol, W. G. J. *FEBS Lett.* **2004**, *577*, 315.
(2) Crans, D. C.; Smee, J.; Gaidamauskas, E.; Yang, L. *Chem. Rev.* **2004**, *104*, 849.
(3) Kornberg, A.; Baker, T. A. *DNA Replication*; W. H. Freeman: New York, 1992.
(4) Pelletier, H.; Sawaya, M. R.; Kumar, A.; Wilson, S. H.; Kraut, J. *Science* **1994**, *264*, 1891
(5) Doublie, S.; Sawaya, M. R.; Ellenberger, T. *Structure* **1999**, *7*, R31.
(6) Fothergill, M.; Goodman, M. F.; Petruska, J.; Warshel, A. *J. Am. Chem. Soc.* **1995**, *117*, 11619.
(7) Florián, J.; Goodman, M. F.; Warshel, A. *J. Am. Chem. Soc.* **2003**, *125*, 8163.
(8) Bunton, C. A.; Llewellyn, D. R.; Oldham, K. G.; Vernon, C. A. *J. Chem. Soc.* **1958**, 3574.
(9) Hu, C.-H.; Brinck, T. *J. Phys. Chem. A* **1999**, *103*, 5379.
(10) Bianciotto, M.; Barthelat, J. C.; Vigroux, A. *J. Am. Chem. Soc.* **2002**, *124*, 7573.
(11) Lad, C.; Williams, N. H.; Wolfenden, R. *Proc. Natl. Acad. Sci. U.S.A.* **2003**, *100*, 5607.
(12) Thatcher, G. R. J.; Kluger, R. *Adv. Phys. Org. Chem.* **1989**, *25*, 99.
(13) Cleland, W. W.; Hengge, A. C. *FASEB J.* **1995**, *9*, 1585.
(14) Florián, J.; Åqvist, J.; Warshel, A. *J. Am. Chem. Soc.* **1998**, *120*, 11524.
(15) Florián, J.; Warshel, A. *J. Am. Chem. Soc.* **1997**, *119*, 5473.
(16) Aqvist, J.; Kolmodin, K.; Florian, J.; Warshel, A. *Chem. Biol.* **1999**, *6*, R71.
(17) Florián, J.; Warshel, A. *J. Phys. Chem. B* **1998**, *102*, 719.
(18) Wolfenden, R.; Ridgway, C.; Young, G. *J. Am. Chem. Soc.* **1998**, *120*, 833.
(19) Schroeder, G. K.; Lad, C.; Wyman, P.; Williams, N. H.; Wolfenden, R. *Proc. Natl. Acad. Sci. U.S.A.* **2006**, *103*, 4052.
(20) Uchimaru, T.; Tsuzuki, S.; Storer, W.; Tanabe, K.; Taira, K. *J. Org. Chem.* **1994**, *59*, 1835.
(21) Taira, K.; Uchimaru, T.; Tanabe, K.; Uebayasi, M. *Nucleic Acids Res.* **1991**, *19*, 2747.
(22) Uchimaru, T.; Tanabe, K.; Nishikawa, S.; Taira, K. *J. Am. Chem. Soc.* **1991**, *113*, 4351.
(23) Kirby, A. J.; Younas, M. *J. Chem. Soc. B* **1970**, 510.
(24) Perreault, D. M.; Anslyn, E. V. *Angew. Chem., Int. Ed. Engl.* **1997**, *36*, 432.
(25) Abashkin, Y. G.; Erickson, J. W.; Burt, S. K. *J. Phys. Chem. B* **2001**, *105*, 287.
(26) Lindquist, R. N.; Lynn, J. L., Jr.; Lienhard, G. E. *J. Am. Chem. Soc.* **1973**, *95*, 8762.
(27) Stankiewicz, P. J.; Gresser, M. J. *Biochemistry* **1988**, *27*, 206.
(28) Van Etten, R. L.; Waymack, P. P.; Rehkop, D. M. *J. Am. Chem. Soc.* **1974**, *96*, 6782.
(29) Messmore, J. M.; Raines, R. T. *J. Am. Chem. Soc.* **2000**, *122*, 9911.
(30) Leon-Lai, C. H.; Gresser, M. J.; Tracey, A. S. *Can. J. Chem.* **1996**, *74*, 38.
(31) Gresser, M. J.; Tracey, A. S.; Stankiewicz, P. J. *Adv. Protein Phosphatases* **1987**, *4*, 35.
(32) Dejaegere, A.; Liang, X.; Karplus, M. *J. Chem. Soc., Faraday Trans.* **1994**, *90*, 1763.
(33) Jenkins, L. A.; Bashkin, J. K.; Pennock, J. D.; Florian, J.; Warshel, A. *Inorg. Chem.* **1999**, *38*, 3215.
(34) Takeda, N.; Shibata, M.; Tajima, N.; Hirao, K.; Komiyama, M. *J. Org. Chem.* **2000**, *65*, 4391.
(35) Lopez, X.; York, D. M.; Dejaegere, A.; Karplus, M. *Int. J. Quantum Chem.* **2002**, *86*, 10.
(36) Chen, X.; Zhang, C.-G. *J. Phys. Chem. A* **2004**, *108*, 6407.
(37) Iche-Tarrat, N.; Barthelat, J.-C.; Rinaldi, D.; Vigroux, A. *J. Phys. Chem. B* **2005**, *109*, 22570.
(38) Liang, C.; Ewig, C. S.; Stouch, T. R.; Hagler, A. T. *J. Am. Chem. Soc.* **1993**, *115*, 1537.
(39) Florián, J.; Baumruk, V.; Strajbl, M.; Bednarova, L.; Stepanek, J. *J. Phys. Chem.* **1996**, *100*, 1559.
(40) Florián, J.; Strajbl, M.; Warshel, A. *J. Am. Chem. Soc.* **1998**, *120*, 7959.
(41) Mennucci, B.; Cances, E.; Tomasi, J. *J. Phys. Chem. B* **1997**, *101*, 10506.
(42) Becke, A. D. *J. Chem. Phys.* **1993**, *98*, 5648.
(43) Lee, C.; Yang, W.; Parr, R. G. *Phys. Rev. B* **1988**, *37*, 785.
(44) Schafer, A.; Horn, H.; Ahlrichs, R. *J. Chem. Phys.* **1992**, *97*, 2571.
(45) Frisch, M. J.; Trucks, G. W.; Schlegel, H. B.; Scuseria, G. E.; Robb, M. A.; Cheeseman, J. R.; Montgomery, J. A., Jr.; Vreven, T.; Kudin, K. N.; Burant, J. C.; Millam, J. M.; Iyengar, S. S.; Tomasi, J.; Barone, V.; Mennucci, B.; Cossi, M.; Scalmani, G.; Rega, N.; Petersson, G. A.; Nakatsuji, H.; Hada, M.; Ehara, M.; Toyota, K.; Fukuda, R.; Hasegawa, J.; Ishida, M.; Nakajima, T.; Honda, Y.; Kitao, O.; Nakai, H.; Klene, M.; Li, X.; Knox, J. E.; Hratchian, H. P.; Cross, J. B.; Bakken, V.; Adamo, C.; Jaramillo, J.; Gomperts, R.; Stratmann, R. E.; Yazyev, O.; Austin, A. J.; Cammi, R.; Pomelli, C.; Ochterski, J. W.; Ayala, P. Y.; Morokuma, K.; Voth, G. A.; Salvador, P.; Dannenberg, J. J.; Zakrzewski, V. G.; Dapprich, S.; Daniels, A. D.; Strain, M. C.; Farkas, O.; Malick, D. K.; Rabuck, A. D.; Raghavachari, K.; Foresman, J. B.; Ortiz, J. V.; Cui, Q.; Baboul, A. G.; Clifford, S.; Cioslowski, J.; Stefanov, B. B.; Liu, G.; Liashenko, A.; Piskorz, P.; Komaromi, I.; Martin, R. L.; Fox, D. J.; Keith, T.; Al-Laham, M. A.; Peng, C. Y.; Nanayakkara, A.; Challacombe, M.; Gill, P. M. W.; Johnson, B.; Chen, W.; Wong, M. W.; Gonzalez, C.; Pople, J. A. *Gaussian 03*, revision C.02; Gaussian, Inc.: Wallingford, CT, 2004.
(46) Kuhn, B.; Kollman, P. A. *J. Am. Chem. Soc.* **2000**, *122*, 2586
(47) Strajbl, M.; Florián, J.; Warshel, A. *J. Phys. Chem. B.* **2001**, *105*, 4471.
(48) Jencks, W. P. *Catalysis in Chemistry and Enzymology*; Dover Publications: New York, 1987.
(49) Strajbl, M.; Florián, J.; Warshel, A. *J. Am. Chem. Soc.* **2000**, *122*, 5354.
(50) Florián, J.; Warshel, A. *J. Am. Chem. Soc.* **1997**, *119*, 5473.
(51) Peräkylä, M.; Kollman, P. A. *J. Phys. Chem. A* **1999**, *103*, 8067.
(52) Bakowies, D.; Kollman, P. A. *J. Am. Chem. Soc.* **1999**, *121*, 5712.
(53) Florián, J.; Warshel, A. *J. Phys. Chem. B* **1999**, *103*, 10282.
(54) Florián, J.; Warshel, A. *J. Phys. Chem. B* **1997**, *101*, 5583.
(55) Alagona, G.; Ghio, C.; Kollman, P. *J. Am. Chem. Soc.* **1983**, *105*, 5226.
(56) Frey, P. A.; Sammons, R. D. *Science* **1985**, *228*, 541

(57) Alber, F.; Folkers, G.; Carloni, P. *J. Phys. Chem. B* **1999**, *103*, 6121.
(58) Kyogoku, Y.; Iitaka, Y. *Acta Crystallogr.* **1966**, *21*, 49.
(59) Mayaan, E.; Range, K.; York, D. M. *J. Biol. Inorg. Chem.* **2004**, *9*, 807.
(60) Klooster, W. T.; Craven, B. M. *Acta Crystallogr., Sect. C: Cryst. Struct. Commun.* **1992**, *48*, 19.
(61) Giarda, L.; Garbassi, F.; Calcaterra, M. *Acta Crystallogr., Sect. B: Struct. Crystallogr. Cryst. Chem.* **1973**, *29*, 1826.
(62) Ezra, F. S.; Collin, R. L. *Acta Crystallogr., Sect. B: Struct. Crystallogr. Cryst. Chem.* **1973**, *29*, 1398.
(63) Hikichi, S.; Tanaka, M.; Morooka, Y.; Kitajima, N. *J. Chem. Soc., Chem. Commun.* **1992**, 814.
(64) Viswamitra, M. A.; Reddy, B. S.; James, M. N. G.; Williams, G. J. B. *Acta Crystallogr., Sect. B: Struct. Crystallogr. Cryst. Chem.* **1972**, *28*, 1108.
(65) Hoogendorp, J. D.; Romers, C. *Acta Crystallogr., Sect. B: Struct. Crystallogr. Cryst. Chem.* **1978**, *34*, 2724.
(66) Newton, G. M.; Cox, J. R., Jr.; Bertrand, J. A. *J. Am. Chem. Soc.* **1966**, *88*, 1503.
(67) Henderson, R. A.; Hughes, D. L.; Janas, Z.; Richards, R. L.; Sobota, P.; Szafert, S. *J. Organomet. Chem.* **1998**, *554*, 195.
(68) Angus-Dunne, S. J.; Batchelor, R. J.; Tracey, A. S.; Einstein, F. W. B. *J. Am. Chem. Soc.* **1995**, *117*, 5292.
(69) Rosenthal, E. C. E.; Girgsdies, F. Z. *Z. Anorg. Allg. Chem.* **2002**, *628*, 1917.
(70) Toscano, P. J.; Schermerhorn, E. J.; Dettelbacher, C.; Macherone, D.; Zubieta, J. *J. Chem. Soc., Chem. Commun.* **1991**, 933.
(71) Crans, D. C.; Felty, R. A.; Anderson, O. P.; Miller, M. M. *Inorg. Chem.* **1993**, *32*, 247.
(72) Feher, F. J.; Walzer, J. F. *Inorg. Chem.* **1991**, *30*, 1689.
(73) Crans, D. C.; Felty, R. A.; Miller, M. M. *J. Am. Chem. Soc.* **1991**, *113*, 265.
(74) Hillerns, F.; Olbrich, F.; Behrens, U.; Rehder, D. *Angew. Chem., Int. Ed. Engl.* **1992**, *31*, 447.
(75) Priebsch, W.; Rehder, D. *Inorg. Chem.* **1990**, *29*, 3013.
(76) Caughlan, C. N.; Smith, H. M.; Watenpaugh, K. *Inorg. Chem.* **1966**, *5*, 2131.
(77) Caravan, P.; Gelmini, L.; Glover, N.; Herring, F. G.; Li, H.; McNeill, J. H.; Rettig, S. J.; Setyawati, I. A.; Shuter, E.; Sun, Y.; Tracey, A. S.; Yuen, V. G.; Orvig, C. *J. Am. Chem. Soc.* **1995**, *117*, 12759.
(78) Jiang, F.; Anderson, O. P.; Miller, S. M.; Chen, J.; Mahroof-Tahir, M.; Crans, D. C. *Inorg. Chem.* **1998**, *37*, 5439.
(79) Cornell, W. D.; Cieplak, P.; Bayly, C. I.; Gould, I. R.; Merz, K. M., Jr.; Ferguson, D. M.; Spellmeyer, D. C.; Fox, T.; Caldwell, J. W.; Kollman, P. A. *J. Am. Chem. Soc.* **1995**, *117*, 5179.
(80) Herschlag, D.; Piccirilli, J. A.; Cech, T. R. *Biochemistry* **1991**, *30*, 4844.
(81) Williams, N. H.; Wyman, P. *Chem. Commun.* **2001**, 1268.
(82) Williams, N. H.; Cheung, W.; Chin, J. *J. Am. Chem. Soc.* **1998**, *120*, 8079.
(83) Florián, J.; Goodman, M. F.; Warshel, A. *Biopolymers* **2003**, *68*, 286.
(84) Rinaldi, D.; Rivail, J.-L. *Theor. Chim. Acta* **1973**, *32*, 57.
(85) Curutchet, C.; Cramer, C. J.; Truhlar, D. G.; Ruiz-Lopez, M. F.; Rinaldi, D.; Orozco, M.; Luque, F. J. *J. Comput. Chem.* **2003**, *24*, 284.
(86) Eyring, H. *Chem. Rev.* **1935**, *17*, 65.
(87) Guthrie, J. P. *J. Am. Chem. Soc.* **1977**, *99*, 3992.
(88) Kumamoto, J.; Cox, J. R., Jr.; Westheimer, F. H. *J. Am. Chem. Soc.* **1956**, *78*, 4858.
(89) Bunton, C. A.; Mhala, M. M.; Oldham, K. G.; Vernon, C. A. *J. Chem. Soc.* **1960**, 3293.
(90) Krauss, M.; Basch, H. *J. Am. Chem. Soc.* **1992**, *114*, 3630.
(91) Wladkowski, B. D.; Svensson, L. A.; Sjolin, L.; Ladner, J. E.; Gilliland, G. L. *J. Am. Chem. Soc.* **1998**, *120*, 5488.
(92) Lowry, T. H.; Richardson, K. S. *Mechanism and Theory in Organic Chemistry*; Harper Collins Publishers: New York, 1987.
(93) Wolfenden, R. *Nature* **1969**, *223*, 704.
(94) Wolfenden, R.; Snider, R. J. *Acc. Chem. Res.* **2001**, *34*, 938.
(95) Bakhtina, M.; Lee, S.; Wang, Y.; Dunlap, C.; Lamarche, B.; Tsai, M. D. *J. Am. Chem. Soc.* **2005**, *44*, 5177.
(96) Florián, J.; Warshel, A. *Phosphorus, Sulfur Silicon Relat. Elem.* **1999**, *144*−*146*, 525.
(97) Gresser, M. J.; Tracey, A. S. *J. Am. Chem. Soc.* **1985**, *107*, 4215.
(98) Raines, R. T. *Chem. Rev.* **1998**, *98*, 1045.
(99) Hambley, T. W.; Judd, R. J.; Lay, P. A. *Inorg. Chem.* **1992**, *31*, 343.
(100) Crans, D. C.; Shin, P. K. *Inorg. Chem.* **1988**, *27*, 1797.
(101) Crans, D. C.; Ehde, P. M.; Shin, P. K.; Pettersson, L. *J. Am. Chem. Soc.* **1991**, *113*, 3728.
(102) Cornman, C. R.; Kampf, J.; Lah, M. S.; Pecoraro, V. L. *Inorg. Chem.* **1992**, *31*, 2035.
(103) Crans, D. C.; Shin, P. K. *J. Am. Chem. Soc.* **1994**, *116*, 1305.
(104) Colpas, G. J.; Hamstra, B. J.; Kampf, J. W.; Pecoraro, V. L. *J. Am. Chem. Soc.* **1996**, *118*, 3469.
(105) Crans, D. C.; Boukhobza, I. *J. Am. Chem. Soc.* **1998**, *120*, 8069.
(106) Crans, D. C.; Simone, C. M.; Blanchard, J. S. *J. Am. Chem. Soc.* **1992**, *114*, 4927.
(107) Crans, D. C.; Marshman, R. W.; Nielsen, R.; Felty, I. *J. Org. Chem.* **1993**, *58*, 2244.
(108) Keramidas, A. D.; Papaioannou, A. B.; Vlahos, A.; Kabanos, T. A.; Bonas, G.; Makriyannis, A.; Raptopoulou, C. P.; Terzis, A. *Inorg. Chem.* **1996**, *35*, 357.
(109) Pessoa, J. C.; Duarte, M. T.; Gillard, R. D.; Madeira, C.; Matias, P. M.; Tomaz, I. *J. Chem. Soc., Dalton Trans.* **1998**, 4015.
(110) Kiss, T.; Petrohan, K.; Buglyo, P.; Sanna, D.; G., M.; Costa Pessoa, J.; Madeira, C. *Inorg. Chem.* **1998**, *37*, 6389.
(111) Crans, D. C.; Schelble, S. M.; Theisen, L. A. *J. Org. Chem.* **1991**, *56*, 1266.
(112) Klamt, A.; Schuurmann, G. *J. Chem. Soc., Perkin Trans. 2* **1993**, 799.